THE ASTROPHYSICAL JOURNAL, 243:625–640, 1981 January 15

ROTATION IN SOLAR-TYPE STARS. I. EVOLUTIONARY MODELS FOR THE SPIN-DOWN OF THE SUN[1]

A. S. ENDAL[2]
Department of Physics and Astronomy, Louisiana State University
AND
S. SOFIA
Laboratory for Planetary Atmospheres, NASA Goddard Space Flight Center
Received 1980 May 27; accepted 1980 August 8

ABSTRACT

We have calculated models of rotating 1 $M_\odot$ stars through the pre–main-sequence and main-sequence stages. The calculations start on the Hayashi track with rapid, rigid-body rotation. As the models evolve, angular momentum is removed from the convective envelope to simulate the effect of the solar wind. In the interior, angular momentum redistribution by circulation flows and rotational instabilities is computed by a diffusion technique developed in earlier papers.

The evolution has been followed up to the present age of the Sun for several values of the initial rotation rate. We find that our solar-age models have internal rotation rates significantly larger than allowed by the measured solar oblateness. Examination of our results suggests that we have *underestimated* the effects of circulation currents near the outer boundary of the radiative interior.

An important result of this study is that circulation currents produce deep mixing of certain minor constituents (^{3}He, ^{13}C, etc.). Such mixing explains the low $^{12}C/^{13}C$ ratios found in solar-type stars which have evolved to the red giant branch. It may also explain the observed steady depletion of lithium during the main-sequence stage.

Subject headings: convection — stars: evolution — Sun: interior — Sun: rotation

I. INTRODUCTION

The question of the internal rotation of the Sun has arisen in a variety of physical and astrophysical contexts of fundamental importance. We shall not attempt to provide here a complete list of the problems where solar internal rotation is relevant. Instead, we will concentrate on those problems which are most prominent at the present time.

The external gravitational field of the rotating Sun has a nonzero quadrupole moment, of amplitude J_2. The magnitude of J_2 is determined by the rotation rate and mass distribution within the Sun. Since the quadrupole moment affects the motions of bodies in the solar system, J_2 can, in principle, be determined from these motions. In practice, the perturbations are difficult to measure and must be interpreted in terms of a specific theory of gravity, so only limits on J_2 are presently available. For example, within Newtonian physics, the 43″ per century advance of the perihelion of Mercury could be caused by a large quadrupole moment ($J_2 \approx 3.3 \times 10^{-4}$). However, this would also produce an unacceptably large rate of change of the inclination of the orbit (Shapiro 1965); consequently, no more than 20% of the perihelion advance could be consistently attributed to the solar quadrupole moment. This provides a firm upper limit: $J_2 \lesssim 6.6 \times 10^{-5}$. On the other hand, the full amount of the perihelion advance (to the accuracy of the observations) is predicted by Einstein's general theory of relativity, with a negligible quadrupole moment contribution. This has historically been interpreted as both proving the accuracy of Einstein's theory and showing that J_2 is very small. In the context of Einstein's theory, the available data on Mercury's orbit give $J_2 = (2.4 \pm 1.7) \times 10^{-6}$ (Anderson *et al.* 1978). The quoted error refers to 1 σ, so the deviation from zero is not significant.[3]

[1]Contribution of the Louisiana State University Observatory No. 160.

[2]Supported in part by National Science Foundation grants AST78-23325 and AST79-19688.

[3]Recent attempts to set limits on J_2, more independently of Einstein's theory, have interpreted planetary and lunar motions in terms of the general class of metric gravitational theories represented by the parametrized post-Newtonian (PPN) formalism (Will and Nordtvedt 1972). For the restricted class of theories in which only the Eddington-Robertson parameters (β, γ) deviate from zero, Williams *et al.* (1976) derive $J_2 \leq 6 \times 10^{-6}$, while Anderson *et al.* (1978) find $J_2 = (-0.3 \pm 4.1) \times 10^{-6}$. These restrictions apply to the scalar-tensor theory of Brans and Dicke (1961), as well as to Einstein's theory. However, these values do not apply to certain other theories, such as that of Rosen (1971). Furthermore, the analysis of the lunar ranging experiment (used in deriving these values) assumed that the solar quadrupole moment is due to uniform rotation (see N. 27 of Shapiro, Counselman, and King 1976). Caution must be exercised when applying these results to a study of solar internal rotation.

For given distributions of solar surface velocities and magnetic fields, J_2 is uniquely related to the solar surface oblateness:

$$\varepsilon = (R_{eq} - R_{pole})/R, \quad (1)$$

where R_{eq} and R_{pole} are the equatorial and polar radii and R is the mean. For the case of uniform surface rotation (angular velocity ω_s) and negligible magnetic fields,

$$\varepsilon = \frac{3}{2}J_2 + \frac{1}{2}\omega_s{}^2 R/g, \quad (2)$$

where g is the surface gravity. Over a decade ago, Dicke and Goldenberg (1976) announced the detection of the solar oblateness, with a value of $(5.0 \pm 0.7) \times 10^{-5}$, corresponding to $J_2 = (2.6 \pm 0.4) \times 10^{-5}$. From this, they concluded that 8% of the Mercury perihelion advance is produced by the solar quadrupole moment and that the prediction of Einstein's theory is too large by this amount. This was used in support of the scalar-tensor theory of gravitation. More recently, the oblateness measurement has been questioned by Hill and Stebbins (1975), who obtained a much smaller value of $\varepsilon = (9.6 \pm 6.5) \times 10^{-6}$. This is consistent with uniform rotation throughout the interior and would make the quadrupole moment contribution to Mercury's orbit negligible. Because the quadrupole moment is a potentially important test both of general relativity and of the internal rotation and mass distribution of the Sun, an accurate measurement would be of great value. In the future, such a measurement could be provided by a Solar Probe mission (see Neugebauer and Davies 1978).

A second problem which *may* be related to rotation concerns the discrepancy between the predicted and observed values of the solar neutrino flux. The model predictions hover around 5 solar neutrino units (SNU) (cf. Bahcall 1978), while the observed flux is 1.6 ± 0.4 SNU (Davis 1978). The resolution of this discrepancy may require a revision of the nuclear reaction rates in the *pp* chain, some entirely new type of physical process (e.g., neutrino oscillations), or a fundamental revision of the theory of stellar evolution. However, the discrepancy could also be due to internal rotation: a rapidly rotating core would reduce the central temperature and therefore the neutrino emission rate (cf. Demarque, Mengel, and Sweigert 1973). Such a solution is contrained by the limits on J_2 and ε (the Demarque *et al.* models violate these constraints), but it is not necessarily true that a rotational solution of the neutrino problem and a small surface distortion are mutually exclusive. The neutrino flux is entirely determined by the conditions near the center of the Sun, while J_2 and ε are largely determined by the rotation at some distance from the center. Thus, a small, rapidly rotating core could solve the neutrino problem without producing a large surface distortion (see § IV*b*). Whether such rapid core rotation is dynamically stable and justifiable from a stellar evolution viewpoint is a major question to be adressed by the current investigation.

A third area of interest concerns the mechanisms which transport angular momentum within the Sun and, in general, the fluid dynamics of the solar interior. A variety of observations (see § II*a*) show that the surface rotation rate has decreased significantly during the lifetime of the Sun. This is presumably due to the torque exerted on the surface layers by the solar wind (cf. Brandt 1966). The central question here is how this braking will affect the interior rotation. This question must, of course, be answered in order to address the first two problems, but it also has intrinsic interest of its own. By using the observational constraints on J_2 and ε, and additional data obtainable from solar oscillation studies (Wolff 1976; Rhodes, Deubner, and Ulrich 1979), we can test various models for the internal angular momentum flows and associated fluid dynamics of the solar interior. In this sense, rotation can be used as a diagnostic tool to study the physics of the solar interior.

In this paper, we describe some initial attempts at simulating the history of the rotating Sun. We have treated this simulation as an initial value problem, starting with a prescribed internal rotation in a fully convective, pre–main-sequence model. These initial conditions are discussed in § II. The evolution of this model is then followed to the present age of the Sun, using the nonspherical stellar structure code of Endal and Sofia (1976). During this evolution, angular momentum is removed from the surface layers at the rate indicated by the solar wind equations (Belcher and MacGregor 1976). Angular momentum redistribution within the interior is treated as a turbulent diffusion process, as described in § III.

The results of several simulations with different initial conditions (total angular momentum) are described and summarized in §§ IV and V. Some computational considerations are discussed in Appendices.

II. INITIAL CONDITIONS

a) *The Initial Rotation*

The conventional starting point for a stellar evolution calculation is a chemically homogeneous, zero-age main-sequence (ZAMS) model. This is reasonable because the main sequence is the first stage at which the chemical composition is significantly altered by nuclear reactions. Thus, the only physical parameters which need to be specified are the total mass and (uniform) chemical composition. According to the Vogt-Russell theorem, this ensures a unique static solution (see, however, Appendix A). For an investigation of the rotational history of the Sun, however, this is not

sufficient because the total angular momentum and internal distribution of angular momentum must also be specified, and these quantities are determined by the evolution prior to reaching the ZAMS.

An obvious alternative would be to begin with the dense interstellar cloud from which the Sun formed, but this is impractical for two reasons. First, it requires input physics and computational techniques which are very different from those employed in stellar evolution calculations; second, this stage is fraught with uncertainties which are all too well known in the field of star formation (Buff, Gerola, and Stellingwerf 1979). A better choice may be to begin the evolution while the star is on the pre–main-sequence Hayashi track, in a fully convective state. Because of the homogenizing nature of convection, the internal distribution of angular momentum will be radically altered during this stage, and the only parameter which will be "remembered" from the earlier stages is the total angular momentum. It should be stated at this time that the assumption that the Sun goes through a fully convective stage may be questioned, since Larson's (1969) calculations of star formation suggest that the convective envelope, at its maximum depth, includes only 57% of the total mass (in a 1 $M_\odot$ star). As noted above, there are major uncertainties in such calculations, and recent observational studies of pre–main-sequence stars appear to contradict these results (Cohen and Kuhi 1979). While this question should be kept in mind, we feel that the assumption of a fully convective starting model is reasonable at this stage in our investigation.

Determining the angular momentum distribution which results from convection is far from trivial, though limiting cases can be assigned. First, for adiabatic convection, the angular velocity must be a function only of the distance ($\tilde{\omega}$) from the rotation axis by virtue of the Taylor-Proudman theorem for barytropic fluids. Adiabatic convection should be an excellent approximation for most of the interior and this severely restricts the possible rotation laws. If the convection is laminar and magnetic fields are not dynamically significant, then convective elements will conserve their initial angular momentum until they merge with the ambient medium. The result of this type of convection will be a uniform distribution of specific angular momentum, i.e., $\omega \propto \tilde{\omega}^{-2}$. This forms one limiting case. On the other hand, stellar convection is not laminar, and this will give rise to an enhanced turbulent eddy viscosity. If this viscosity is dominant and isotropic, it will produce rigid-body rotation, i.e., ω = constant, and this forms the second limiting case. Convective motions occur preferentially along directions parallel to the gravitational acceleration and, in the "molecular viscosity" picture, this gives rise to an anisotropic viscosity (cf. Kippenhahn 1963). This will lead to departures from the ω = constant case. Although preliminary steps have been made toward formulating a theory of turbulent viscosity (cf. Durney and Spruit 1979), the theory is not yet developed to the point where actual predictions can be made. However, it appears that the rotation law produced by convection should lie between the two limiting cases. For the calculations described in this paper, we have used the ω = constant case (rigid-body rotation) in the initial model and in any convection zones appearing in later models. The uniform specific angular momentum case will be explored in a subsequent paper. By calculating both cases and comparing the results to the observational data on the present Sun, it should be possible to determine which case is most nearly correct and, thereby, gain a better understanding of the interaction of rotation with convection.

The next step is to choose an appropriate total angular momentum for the initial model. In this case, there are considerable observational data which can be used as a guide. The observed rotational velocities of main-sequence stars can be used to form a relationship between the mean velocity at a given spectral type and the corresponding mass M. Kraft (1970) has pointed out that, if this is converted into a relationship between total angular momentum (assuming rigid-body rotation) and mass, the result is a simple power law for those stars more massive than 1.5 $M_\odot$. From Kraft's Figure 3, we can write this relationship as

$$\langle J \rangle / J_\odot = 61.5\,(M/M_\odot)^{1.57} \quad \text{for} \quad M/M_\odot > 1.5, \tag{3}$$

where $\langle J \rangle$ is the mean total angular momentum for stars of a given mass and

$$J_\odot = 2.0 \times 10^{48}\ \mathrm{g\,cm^2\,s^{-1}}$$

is the present angular momentum of the Sun, if the interior rotates at the same rate as the surface layers. There is a break in this relationship at $\sim$1.5 $M_\odot$, with the less massive stars rotating much more slowly than indicated by equation (3). The break coincides with the transition from shallow to deep surface convection zones (Demarque and Roeder 1967), and the slow rotation of the low-mass stars is generally attributed to rotation braking by magnetically coupled stellar (solar) winds. According to Durney and Latour (1978), a deep convective envelope is a necessary condition for generating the required magnetic field. In this case, the massive stars reflect the true distribution of initial angular momenta, and we may use equation (3) to infer the initial angular momentum of a typical 1 $M_\odot$ star, i.e., $\langle J(t=0) \rangle = 61.5\ J_\odot$. An analysis by Bernacca and Perinotto (1974), based on more extensive data, gives $\langle J(t=0) \rangle \approx 70\ J_\odot$, in reasonable agreement with the first estimate. Furthermore, the rapid rotation of solar-type stars in young clusters suggests that most of the angular momentum is lost during the main-sequence

stage so we may use equation (3) to specify the angular momentum of our initial (pre–main-sequence) model.

Finally, we should bear in mind that there is no guarantee that the Sun's rotation is typical for a star of the solar mass and age. Indeed, there is some controversy on this point (Skumanich 1972; Smith 1980). For this reason, we have calculated three sequences, with initial angular momenta equal to 3, 1, and 1/3 times the value given by equation (3).

b) *Construction of the Initial Models*

The initial models were constructed by a method similar to that of Iben (1965), which takes advantage of the fully convective nature of the star at this point. Briefly, the starting point was chosen at a central temperature low enough that nuclear reactions could be ignored. In this case the local rate of energy release per gram is

$$\varepsilon_g = \frac{P}{\rho^2}\frac{d\rho}{dt} - \frac{dU}{dt} = -T\frac{ds}{dt}, \qquad (4)$$

where P is the pressure, ρ the density, U the internal energy per gram, T the temperature, and s the specific entropy. Since the convection is nearly adiabatic throughout most of the star, s and ds/dt are essentially constants for a given model. To start a model sequence, two models were constructed with different ds/dt values. Approximate models were obtained by the fitting (integration) technique and improved by Henyey iterations. The model with the larger radius and luminosity corresponds to the earlier time, and the time difference between the models is given by one-half the change in the gravitational energy divided by the average luminosity (rotational energy was not included in the initial models). Subsequent models were computed by the normal Henyey relaxation technique, including rotational effects (Endal and Sofia 1976).

The approximate parameters of the initial models were: $L=25\ L_\odot$ and $R=9\ R_\odot$ at the surface, and $T=10^6$ K and $\rho=10^{-2}$ g cm^{-3} at the center. At this point, the models were fully convective and the evolutionary time scales were sufficiently short that little angular momentum would have been lost during the prior evolution, according to our scaled-up solar wind model (see § III). This last point was checked by starting one sequence at a radius of 90 $R_\odot$ and confirming that no significant angular momentum loss was predicted during the first tenfold decrease in radius.

III. CALCULATION OF THE EVOLUTION

a) *The Solar Wind Model*

In order to allow for angular momentum losses due to the solar wind (the mass loss is negligible), it is necessary to adopt a specific solar wind model. This model must predict the dependence of the angular momentum loss rate on the age of the Sun (or on the rotation rate), as well as the present loss rate, and this involves a number of assumptions, which must be carefully examined. We have adopted the model of Belcher and MacGregor (1976); the primary assumptions in this model are listed and discussed below:

1. The wind is considered to be a one-component, steady-state, axisymmetric flow, as described by the MHD equations of Weber and Davis (1967). As discussed by Belcher and MacGregor, the assumption of axial symmetry becomes questionable when the rotational kinetic energy of the wind is greater than or comparable to the thermal energy input from the convection zone. Assuming a constant thermal energy input (see below), this occurs for rotation rates greater than 5 times the present value, so this is a serious weakness. However, three-dimensional wind models have not, to our knowledge, been developed to the point where they can make the type of predictions we need. Considering the uncertainties in other necessary assumptions, it is doubtful that a three-dimensional model would be warranted.

2. The strength of the magnetic field at the solar surface is assumed to be proportional to the rotation rate. Belcher and MacGregor explored a number of power law dependences. We chose the linear case as best representing the available observations on the correlation between Ca II emission (a magnetic field indicator) and rotation rates (see Skumanich 1972).

3. The total energy of the wind is assumed to equal the sum of the (thermal) input from the convection zone and the rotational energy input. The thermal input is assumed to be constant at its present value ($\sim 10^{27}$ ergs s^{-1}) while the rotational input is taken to be the rate of loss of rotational energy from the Sun, due to the magnetic braking. This component is not constant and varies from 10^{25} ergs s^{-1} for the present rotation rate to 10^{29} ergs s^{-1} in the early stages. This means that mass flux in the wind (predicted by the wind equations) is not constant. This assumption is certainly more reasonable than that of constant total energy and mass flux.

It should be noted that assumptions 2 and 3 do not allow for any effects of changes in the properties of the surface convection zone. The stellar structure calculations predict that the depth of the convection zone varies significantly, particularly during the early stages (see § IV). However, we have no way of directly estimating how this will affect the angular momentum loss rate. In addition, there is significant evidence that magnetic fields contribute to coronal heating. In the Belcher-MacGregor model, this is included in the *constant* thermal energy input. There is an obvious inconsistency here since the magnetic field strength is a

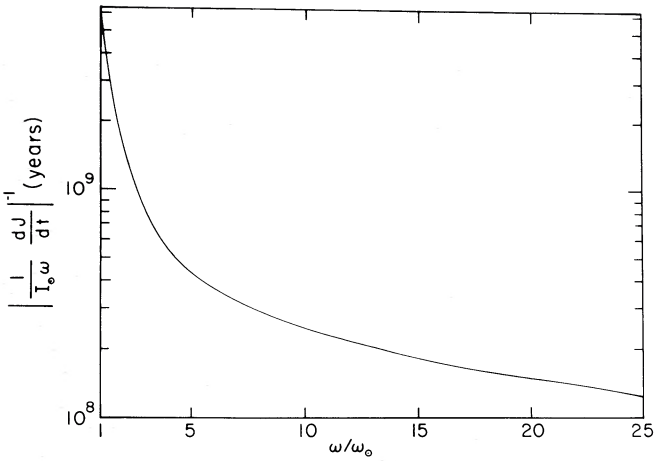

FIG. 1.—Angular momentum loss rate according to the Belcher-MacGregor model of the solar wind. The loss rate is expressed as the *e*-folding time for spin-down of a rigidly rotating star and is shown as a function of the rotation rate (in units of the present surface rotation rate of the Sun).

function of the rotation rate. As a result, the braking torque is underestimated for large rotation rates. The predicted angular momentum loss rate is shown in Figure 1, as a function of the surface rotational velocity.

b) Internal Angular Momentum Flows

In our models, the effect of the solar wind is to decelerate the rotation of the convective envelope, which is assumed to rotate rigidly at the same angular velocity as the surface. The flow of angular momentum within the radiative interior and across the envelope-interior interface was modeled by the techniques of Endal and Sofia (1978). Since these techniques have already been described in detail, we will confine the present description to an outline of the associated physical model.

We assume that, within the radiative interior, the angular velocity is constant on level (constant pressure) surfaces, due to the shear instability (cf. Zahn 1975). Along such a surface, shear turbulence will arise if the Reynolds number

$$\mathrm{Re} = l^2\,\Delta\omega/\nu \qquad (5)$$

is greater than $\mathrm{Re}^{\mathrm{crit}} \approx 10^3$. Here, l is the length scale over which the angular velocity changes by an amount $\Delta\omega$ and ν is the kinematic viscosity (with a typical value of 1 $\mathrm{cm^2\,s^{-1}}$ in the radiative interior). We need not consider the Richardson criterion, since the density stratification along a level surface is negligible. If we evaluate $\Delta\omega$ between the pole and the equator for a shell at radius r, then $l \approx r$. In this case, the criterion for stability is

$$\mathrm{Re} = r^2 f\omega/\nu < \mathrm{Re}^{\mathrm{crit}}, \qquad (6)$$

where f is the fractional change in the angular velocity. Taking $r = \frac{1}{2}R_\odot$ and $\omega = 3\times10^{-6}$ $\mathrm{rad\,s^{-1}}$ (the present surface velocity) gives $f < 3\times10^{-13}$. However, with such a small angular velocity gradient, the time scale for growth of the instability,

$$\tau = \mathrm{Re}^{\mathrm{crit}}/(f\omega), \qquad (7)$$

would be very long ($\sim 4\times10^{13}$ yr). If, as a conservative estimate, we require that the time scale given by equation (7) be greater than one-tenth of the Kelvin time ($\tau_K = 2\times10^7$ yr) in order for the differential rotation to be maintained, we get $f < 6\times10^{-6}$. Since this corresponds to

$$\Delta\omega < 2\times10^{-11}\ \mathrm{rad\,s^{-1}},$$

constant rotation on level surfaces is, in fact, an excellent approximation on all time scales of interest. It should be noted that the instability of Goldreich and Schubert (1967), which would lead to constant rotation on cylinders, cannot compete effectively with the shear instability. The Goldreich-Schubert mechanism specifically depends on thermal relaxation of the perturbation and therefore has a characteristic time scale equal to or greater than the Kelvin time.

Given that the angular velocity is constant on level surfaces, we need only model the angular momentum flows in the vertical (i.e., radial) direction. These flows are first divided into two categories, dynamical and secular, according to the time scales associated with the triggering mechanisms. The dynamical flows result from instability to adiabatic perturbations and therefore are characterized by very short (dynamical) time scales. If such flows arise, they will redistribute the angular momentum very quickly. Thus, the angular velocity gradient should remain dynamically stable on evolu-

tionary time scales. In the models, this was accomplished by instantaneously readjusting the velocity gradient to be marginally stable whenever an instability arose. The shear and Solberg-Hoiland instabilities were handled in this manner; the stability criteria are discussed by Endal and Sofia (1978).

The secular flows (circulation currents) result from thermal instabilities and are characterized by Kelvin time scales. These time scales are comparable to the surface-braking and evolutionary time scales, so instantaneous readjustment is not appropriate. As in the case of convection, the circulation currents can redistribute angular momentum either by laminar advection or through an enhanced turbulent viscosity. In our models, we have *assumed* that the turbulent viscosity dominates and therefore that the angular momentum transport may be described as a diffusion process. This may be partially justified by noting that the Reynolds numbers of the flows are supercritical so turbulence will certainly arise. In addition, laminar advection would lead to inward transport of angular momentum and to a large, rapidly rotating core (Sakurai 1972). This is ruled out by constraints on the present quadrupole moment and surface oblateness of the Sun (see § I).

The diffusion equations used in the present models differ somewhat from those of Endal and Sofia (1978). Specifically, we have added source/sink terms representing contraction/expansion in the angular velocity equation and nuclear reaction terms in the composition equations. These terms were added because their time scales are comparable to the diffusion time, so their effects should be considered in conjunction with diffusion. This is especially important for the nuclear reactions, which can lead to μ-barriers preventing circulation. The resulting equations are

$$\frac{\partial \omega}{\partial t} = \frac{1}{\rho r^4}\frac{\partial}{\partial r}\left[\rho r^4 D(\omega, X_i)\frac{\partial \omega}{\partial r}\right] - \frac{2\omega}{r}\frac{\partial r}{\partial t} \quad (8)$$

for the angular velocity, and

$$\frac{\partial X_i}{\partial t} = \frac{1}{\rho r^2}\frac{\partial}{\partial r}\left[\rho r^2 D(\omega, X_i)\frac{\partial X_i}{\partial r}\right] + \left(\frac{\partial X_i}{\partial t}\right)_{\rm nuc} \quad (9)$$

for the mass fraction X_i of species i, at a fixed mass coordinate. The turbulent diffusion coefficient $D(\omega, X_i)$ was taken to be the product of the *locally evaluated* circulation velocity and the pressure scale height (representing a typical circulation length scale). This definition will be discussed further in § IV. Eddington circulation and the Goldreich-Schubert and thermal-shear instabilities were treated by this method; equations for the associated velocities are given by Endal and Sofia (1978).

Finally, we should note that the scenario described above is restricted to angular momentum transport by fluid flows. Other possible effects, such as angular momentum transport by magnetic fields and nonradial pulsations, are possible. At this stage in the investigation, we feel justified in restricting ourselves to effects which are known to exist and fairly well understood. Alternative angular momentum transport mechanisms will be discussed further in § V.

c) *Calculation of the Stellar Structure*

The evolution of the solar interior structure was calculated by the equipotential technique of Endal and Sofia (1976). This technique includes the effects of rotation on both the mechanical equilibrium and energy equations. The primary assumptions are that rotation does not affect the efficiency of convective energy transport (this could be modified if necessary) and that baroclinic effects (departures of constant density surfaces from constant pressure surfaces) are small. For the rotational velocities encountered in this investigation, such effects are of minor importance. Aside from these assumptions, and approximations made in solving the Poisson equation (see Endal and Sofia 1976), the Newtonian effects of rotation on the stellar evolution equations are treated in a formally exact manner.

The nuclear reaction terms in equation (9) and in the energy generation rate included all three branches of the proton-proton chain and the first (CN) branch of the CNO cycle. The abundances of ^{1}H, ^{3}He, ^{4}He, ^{12}C, ^{13}C, and ^{14}N were explicitly calculated from the modified diffusion equations (eq. [9]), while the abundances of the short-lived nuclei (^{2}H, ^{7}Li, ^{7}Be, ^{8}Be, ^{8}B, ^{13}N, ^{15}N, and ^{15}O) were assumed to have their local equilibrium values. All reaction rates were taken from Fowler, Caughlan, and Zimmerman (1975), with the ^{7}Be (e^-, ν_e)Li^7 rate corrected for bound electrons as described by Bahcall and Moeller (1969).

The opacities and equation of state were calculated from the Los Alamos Astrophysical Opacity Library (Huebner *et al.* 1977), supplemented by low-temperature opacities kindly provided by Dr. N. H. Magee, Jr. (private communication). The metal abundance, by mass, was set at $Z=0.01662$. This is in agreement with the value $Z=0.0180\pm0.0016$ derived from the recent compilation of solar surface abundances by Ross and Aller (1976). The hydrogen abundance and the ratio of the convective mixing length to pressure scale height were chosen by requiring that a nonrotating model match the present solar luminosity and radius at an age of 4.7×10^9 yr (see Appendix A). The derived values were $X=0.7123$ and $\alpha=2.2855$, respectively.

IV. RESULTS

a) *Evolution up to age* $= 4.7\times10^9$ *Years*

Three evolutionary sequences were computed, with initial angular momenta equal to 3.38, 1.00, and 0.33

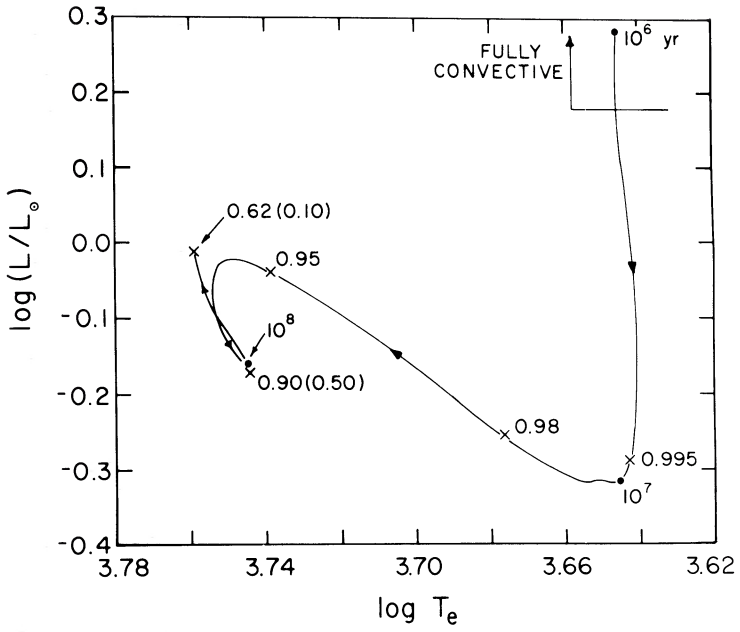

FIG. 2.—H-R diagram for sequence B. The numbers by the heavy dots give the age, in years. The numbers by the ×'s give the fraction of the initial angular momentum remaining in the star; for the last two points (ZAMS and present solar age), the quantity $\omega_s R^2/\omega_i R_i^2$ is given in parentheses.

times the value given by equation (3), for $M=1\ M_\odot$. We will refer to these sequences as A, B, and C, respectively. In describing the evolution, we will concentrate on the intermediate case (sequence B) and discuss the other sequences only when they deviate significantly from sequence B.

The path of sequence B in the theoretical H-R diagram is shown in Figure 2. The high-luminosity portion of the Hayashi track (from $\log L/L_\odot = 1.4$ to 0.3) has been deleted. During the first 10^7 years, the model is on the Hayashi track. Only 0.5% of the initial angular momentum is lost during this period. Solar-wind braking is not significant during the Hayashi phase because the large radius requires that the star rotate very slowly, which, in turn, means that the dynamo-generated magnetic field is very weak.

The model reaches the zero-age main sequence at an age of 4.6×10^7 yr. At this point, it has lost 10% of its initial angular momentum. Since most of this angular momentum has been removed from the convective envelope, the surface rotational velocity is only one-half as large as it would be in the absence of solar-wind braking. The track in Figure 2 (and our calculations) ends at an age of 4.7×10^9 yr, corresponding to the estimated age of the Sun. Although the model retains 62% of its initial angular momentum, very little of this is reflected in the surface rotation rate, which is only 10% of the constant-angular-momentum value. However, the rapid internal rotation does lead to a large surface oblateness—about 35 times the value measured by Hill and Stebbins (1975). This will be discussed further in § IV*b*.

The effect of rotation on the path in the H-R diagram is illustrated in Figure 3, which shows the evolution near the main sequence. The nonrotating ZAMS, displaced in $\log T_e$ by the amount indicated by the horizontal arrow, is also shown. For sequences B and C, rotational effects are of minor importance. However, sequence A (rotating 3 times faster than the norm) is displaced by a substantial amount. Its evolution onto the main sequence corresponds closely to the evolution of a nonrotating model of mass 0.95 $M_\odot$. Photometric (color-magnitude) H-R diagrams are often used to assign ages to stars evolving toward the main sequence, in young clusters (cf. Landolt 1979). Such ages are greater than the nuclear ages based on the evolution of the more massive stars away from the main sequence and this is generally interpreted as evidence for noncoeval star formation. The effects of rotation on such conclusions should be considered; this has previously been explored by Moss (1973), using polytropic models. For stars evolving from the Hayashi track, we find that the age at the ZAMS is 4.46×10^7 yr with no rotation and 4.95×10^7 yr for sequence A (an 11% change); the difference would obviously be greater for more rapid rotation. However, sequence A would be associated with a nonrotating star of mass 0.95 $M_\odot$, based on its position in the H-R diagram. We have calculated such a sequence, starting at our standard point on the Hayashi track, and the age at the ZAMS is 4.89×10^7

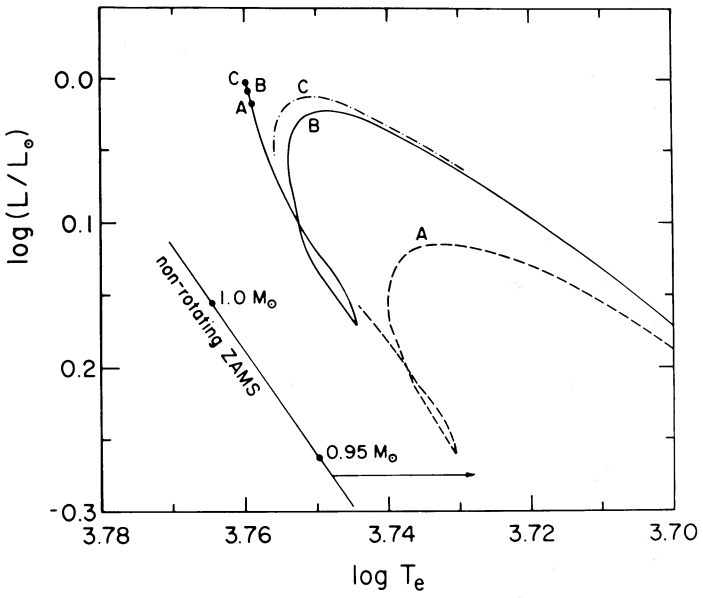

FIG. 3.—The portion of the H-R diagram near the main sequence for sequences A (*dashed line*), B (*solid line*), and C (*dash-dot line*). Parts of the tracks for sequences A and C have been deleted to avoid confusion. Heavy dots indicate the positions at age $=4.7\times10^9$ yr.

yr. This differs from the age of sequence A by only 1%. Thus, there is a cancellation of errors in the age determination between neglecting rotation and assigning the wrong mass, and the photometrically assigned ages should be quite accurate. We find that the effect of rotation on such ages is much smaller than estimated by Moss, using more approximate models.

Figure 4 shows the surface rotational velocities (at the equator) as a function of time. The heavy dots indicate the points at which the models reach the ZAMS. The predicted pre–main-sequence velocities range from 160 km s^{-1} to $\sim$10 km s^{-1}. This agrees with the range of velocities found by Kuhi (1978) for the pre–main-sequence stars in NGC 2264. The dashed lines show the observed relationship between mean rotation velocities and age for solar-type stars, as determined by Skumanich (1972) and Smith (1979). Both lines indicate that the rotational velocity is proportional to (age)$^{-1/2}$. The deviations of our models from this slope are certainly within the observational uncertainties. The Skumanich relationship is based on solar-type stars in young clusters (ages $\lesssim 4\times10^8$ yr) and on the Sun, while Smith's relationship is based on field stars with a broad range of assigned ages. Smith's age estimates are based on the strength of the Ca II K emission line and the lithium abundance. While these parameters certainly do contain age information, there is a danger that the K emission and lithium abundance may be directly influenced by rotation, through the dynamo field strength and rotational mixing, respectively. If Smith's relationship is correct, then the interesting result that the Sun's rotation is slower than

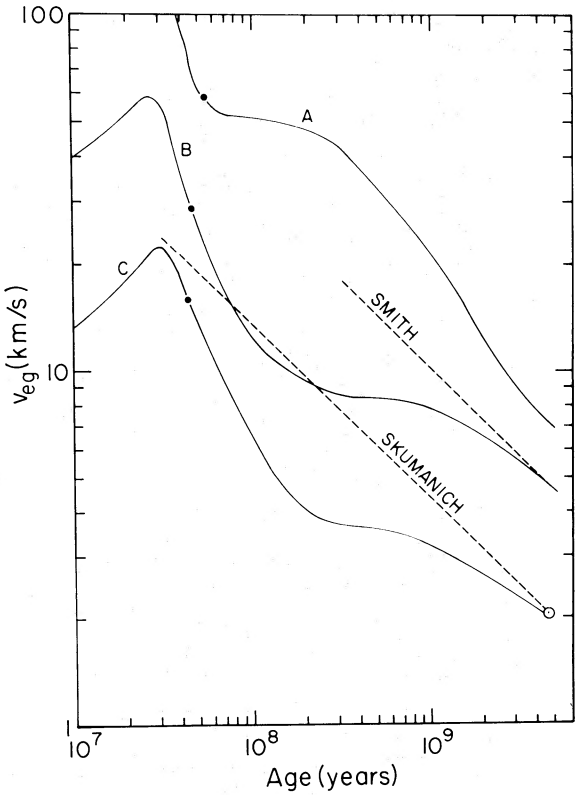

FIG. 4.—Surface rotation velocities at the equator as functions of age for sequences A, B, and C (*solid lines*). The heavy dots indicate the ZAMS stage. The dashed lines show the observed rotation velocity-age relationship for solar-type stars, according to Skumanich (1972) and Smith (1979).

average (by a factor of 2.5) follows. Skumanich's method, which uses the Sun to define the age dependence, could not show such an effect. In fact, our sequence C, which has an initial angular momentum 3 times smaller than the mean given by equation (3), matches the solar surface rotation at an age of 4.7×10^9 yr. However, this should not be construed as strong support for the hypothesis that the Sun is an anomalously slow rotator because our computed velocities are strongly dependent on the assumptions in the solar wind model (see § III*a*).

The development of differential rotation in the stellar interior is illustrated, for sequence B, in Figure 5. Each line shows the angular velocity, as a function of time, at a constant mass coordinate. The corresponding radius coordinate in the model at an age of 4.7×10^9 yr is shown in parentheses. The time interval covered by Figure 5 begins when the star reaches the bottom of the Hayashi track. The line for the surface rotation ($M_r=1.0$) shows that the rotation rate initially increases, as the star contracts toward the ZAMS. The peak rotation rate is reached at an age of 2.8×10^7 yr, i.e., 1.8×10^7 yr prior to reaching the ZAMS (see also Fig. 4). From this point on, angular momentum losses due to the solar wind dominate, and the rotation rate decreases.

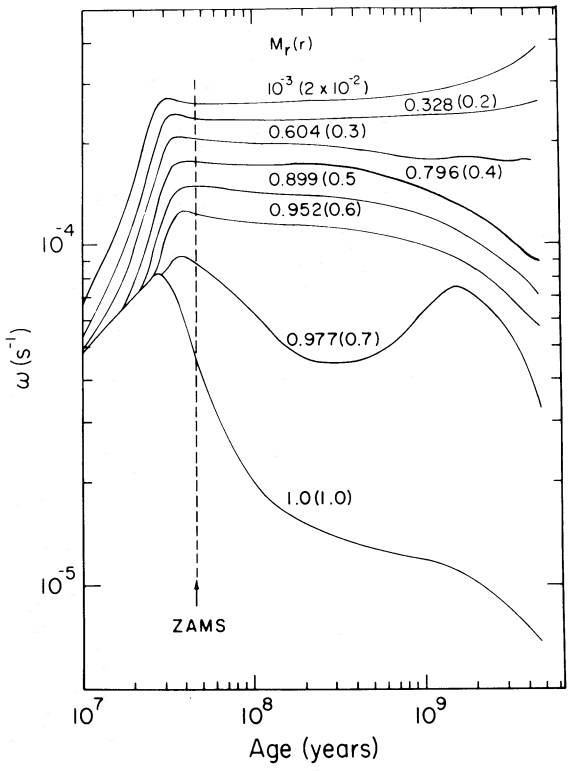

FIG. 5.—Evolution of the internal rotation in the sequence B models. The rotation rates at fixed mass coordinates are shown as functions of time. The lines are labeled by the mass coordinate and (in parentheses) by the radius coordinate of each mass layer in the model at age $=4.7\times10^9$ yr.

The line for the zone nearest the center ($M_r=10^{-3}$) also shows a local peak, at an age of 3.2×10^7 yr. The temporary decrease in the central rotation rate is due to development of a temporary convective core at the onset of (nonequilibrium) nuclear reactions. The convection leads to rigid-body rotation within this core (containing, at its maximum extent, 0.0737 $M_\odot$), and this decreases the angular momentum of the central zone. As a result of the nuclear reactions, a μ-barrier (i.e., a negative gradient of mean molecular weight μ) which inhibits circulation (see Endal and Sofia 1978) is immediately established at the outer edge of this core, and the angular momentum of this region remains constant during the subsequent evolution. The increase in the central zone rotation rate after the ZAMS is due to core contraction as the hydrogen is depleted by nuclear reactions.

The rotation of the intermediate zones is controlled by competition between two mechanisms: core contraction increases the rotation rate of the zones in which the angular momentum is frozen by a μ-barrier while, in the zones not affected by a strong μ-barrier, circulation currents transport angular momentum outward to the convective envelope, where it is removed by the wind. Two transition regions appear in Figure 5. The innermost such region occurs near the $M_r=0.604$ line. This roughly corresponds to the maximum extent of nuclear processing, and therefore to the outer edge of the μ-barrier, in the present Sun. The zones interior to this line increase their rotation rate while the exterior zones slow down. Note that, up to an age of $\sim10^9$ yr, the rotation rate at $M_r=0.604$ decreases, indicating that the μ-barrier has not yet reached this zone. We believe that the outer transition region, near $M_r=0.977$, is an artifact of our local diffusion model, for reasons described below.

b) Internal Rotation and Surface Oblateness at Age $=4.7\times10^9$ Years

The characteristics of our models at the present age of the Sun are summarized in Table 1. The quantities with subscript i refer to initial values, while all other quantities correspond to an age of 4.7×10^9 yr. The quantity $\langle J\rangle_i$ refers to the mean initial angular momentum of a solar type star, as given by equation (3). Sequence O was computed in the same manner as the other sequences, but with the rotation rate set equal to zero.

Most of the quantities in Table 1 vary with the initial rotation rate as expected, but a few of the entries require additional comment. First, note that $1-J/J_i$, the fraction of the initial angular momentum lost during the evolution, increases rapidly with the initial angular momentum. This occurs because the rate of angular momentum loss due to the solar wind increases with the rotation rate (see Fig. 1) and because the more

TABLE 1

MODEL CHARACTERISTICS AT AGE = 4.7×10^9 YEARS

PARAMETER	SEQUENCE			
	A	B	C	O
$J_i/\langle J\rangle_i$	3.38	1.00	0.33	No rotation
$L/L_\odot$	0.940	0.979	0.995	0.9996
$R/R_\odot$	0.981	0.998	1.004	1.0009
$\Sigma(\sigma\nu)$, SNU[a]	3.998	5.483	6.056	6.161
$1-J/J_i$	0.772	0.384	0.186	...
v (surface), km s^{-1}	7.12	4.75	2.00	...
$\omega_{center}/\omega_{surface}$	114	56	45	...
ϵ[b]	9.47×10^{-4}	3.46×10^{-4}	6.38×10^{-5}	...

[a] Neutrino fluxes were calculated using the ^{37}Cl capture cross sections of Bahcall 1978. See the caution about interpreting these values discussed in the text.

[b] The oblateness calculation is described in Appendix B.

rapidly rotating sequences are able to diffuse more of their angular momentum out to the surface, where it can be removed by the solar wind. (The internal circulation velocities increase approximately as the square of the rotation rate; see Endal and Sofia 1980.) In all of our sequences, the effects of rotation are relatively minor at the end of the evolution. This is reflected, for instance, in the nearly uniform luminosities and contrasts sharply with the situation at the ZAMS stage (see Fig. 3). As a result, the increase in the luminosity during the main-sequence stage is much greater for sequence A than for the other sequences (71% vs. ~45%). Finally, we should caution that the neutrino fluxes given in Table 1 should *not* be interpreted as indicating that our present models significantly alleviate the neutrino problem. The low predicted fluxes are primarily due to the slightly lower luminosities of the rotating models. If the initial hydrogen abundances had been adjusted to match the observed solar luminosity, the neutrino fluxes would have been similar to the nonrotating value.

Figure 6 shows the rotation rates, as functions of distance from the center, in the models at age = 4.7×10^9 yr. For sequence B, the regions affected by convection and circulation currents (i.e., Eddington circulation and Goldreich-Schubert instabilities) are also shown. The region where the rotation is stabilized by a μ-barrier extends from the center to the inner boundary of the circulation region, as indicated at the bottom of the figure. The locations of these regions in the sequence A and C models are nearly identical to the locations in the sequence B model, as can be seen by inspection of the rotation curves.

In each model, there is a small, rapidly rotating core (containing ~0.07 $M_\odot$) which rotates 45 to 114 times faster than the surface (see Table 1). This is the region

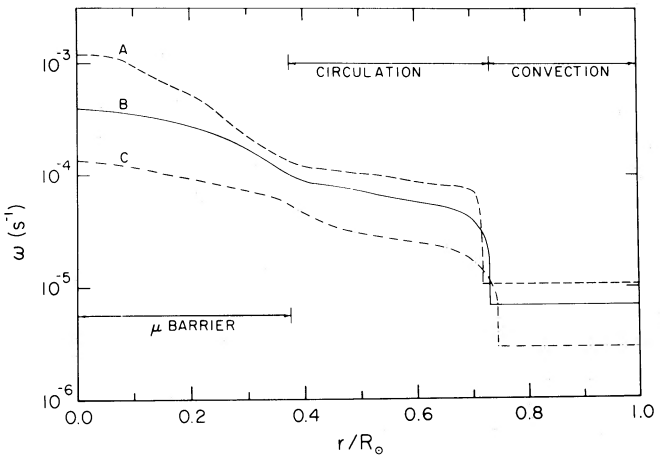

FIG. 6.—Internal rotation rates as functions of the radius coordinate in the models at age = 4.7×10^9 yr. The regions controlled by the μ-barrier, circulation, and convection in the sequence B model are also indicated.

which decoupled from the rest of the model when a convective core formed, near the ZAMS stage (as described in § IV*a*). This core is surrounded by a differentially rotating region through which the μ-barrier moved during the main-sequence stage, as the rotation of the envelope was slowing down. Outside of this region, very little nuclear processing has taken place, so circulation currents are not inhibited by a μ-barrier and a fairly flat rotation curve is maintained. However, the rotation rate in most of the circulation region is nearly an order of magnitude greater than that of the convective envelope (and surface).

Apparently, our present diffusion model is not able to efficiently transport angular momentum from the circulation region into the convective envelope. The isolation of the circulation region from the convective envelope is due to a narrow (radiative) boundary layer in which the rotation rate drops by a factor of ~ 10. Since the circulation velocities are proportional to the square of the rotation rate, the angular momentum diffusion time scale increases by a factor of 100 within this boundary layer. In the sequence B model, for instance, the diffusion time scale (i.e., the characteristic time scale of eq. [8]) increases to 3×10^{11} yr in this region. Therefore, angular momentum cannot be transported across this region. We believe that this isolating boundary layer is an artifact of our diffusion model, which uses circulation velocities computed from the *local* rotation rate. In a *global* circulation model, the circulation patterns should be large compared to the extent of this boundary layer. Continuity conditions would then require that the circulation velocities (and transport time scales) in this layer be comparable to those in the more rapidly rotating interior region. This might prevent the isolation of the circulation region from the convective envelope. Of course, this should be tested by detailed calculations. (The formation of a boundary layer is also responsible for the strange behavior of the $M_r = 0.977$ line in Fig. 5.) We should note that penetration of convective motions into the radiative core will not, in general, remove the isolating boundary layer. Experiments with various depths of convective overshooting showed that such overshooting simply increases the depth at which the boundary layer occurs.

The internal rotation in our models is generally more rapid than in the models derived by Goldreich and Schubert (1968) and Fricke (1969). This is because these authors assumed that development of a secular instability would lead to very rapid angular momentum redistribution. Subsequent investigations have shown that the original estimates of the time scales for angular momentum redistribution were grossly underestimated (Colgate 1968; Kippenhahn 1969; James and Kahn 1970, 1971). In our calculations, which take the longer time scales into account, instabilities can persist for a substantial time. In the models shown in Figure 6, the circulation region is subject to a Goldreich-Schubert instability, and this contributes to angular momentum transport. Here again, the rate of transport is roughly proportional to ω^2 (cf. James and Kahn 1971), so transport is very slow near the outer edge of the circulation region.

The oblateness parameters given in Table 1 are all greater than the value measured by Hill and Stebbins (1975), though the value for sequence C does not differ significantly from that measured by Dicke and Goldenberg (1967). In the following discussion, we adopt the Hill and Stebbins value and consider how much modification of the rotation curves in Figure 6 is required. Since the sequence C model matches the present surface rotation rate of the Sun, we will take this model as most closely representing the Sun.

Our discussion of the local diffusion model suggests that some or all of the circulation region should be rotating at nearly the same rate as the convective envelope. Because the rate of angular momentum loss increases rapidly with the surface rotation rate (see Fig. 1), transfer of part of the angular momentum of the circulation region into the convective envelope would not lead to a large change in the surface rotation rate. To see what effect this would have on the predicted oblateness and to determine how serious the discrepancy between the predicted and observed values is, we performed the following experiments on the rotation curve for model C. The angular velocity of the convective envelope was held fixed. Furthermore, the angular velocity to a specified depth below the convection zone (i.e., to a specified radius coordinate r^*) was also set equal to the surface value. Interior to r^*, the angular velocities were taken from the rotation curve in Figure 6. Figure 7 shows the computed oblateness as a function of r^* (*dashed line*) and as a function of the corresponding M_r^* (*solid line*). The value for $r^* = M_r^* = 0$ is the oblateness for rigid-body rotation. The value measured by Hill and Stebbins and the 1σ and 3σ limits are indicated by horizontal lines.

Even at the 3σ level, it is clear that $r^* \lesssim 0.3\ R_\odot$ ($M_r^* \lesssim 0.6\ M_\odot$) is required if the Hill and Stebbins result is adopted. This sets some fairly severe limits on the rotation curves shown in Figure 6 and requires that the rotation rates in all of the circulation region and part of the μ-barrier region be substantially decreased. However, this does not necessarily require that the μ-barrier be penetrated by the circulation currents since the location of the μ-barrier is a function of time and stronger coupling during the early stages could significantly decrease the rotation rate in the present μ-barrier region. Also these experiments show that, even at the 1σ level, the measured oblateness does not seriously constrain rotational solutions to the neutrino problem. In our nonrotating model, 90% of the neutrino flux is produced interior to $M_r = 0.05\ M_\odot$. The solid curve in Figure 7 shows that the surface oblateness is very

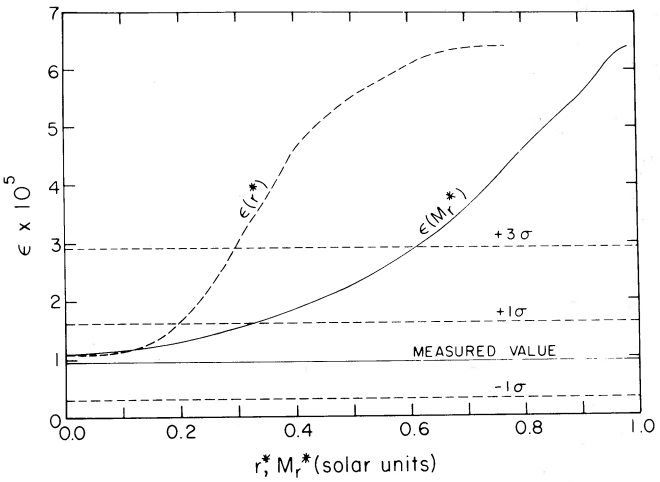

FIG. 7.—The computed oblateness as functions of r^* and M_r^* (see text) for the sequence A model at age $=4.7\times10^9$ yr. The horizontal lines show the solar oblateness (*solid line*) plus 1 and 3σ limits (*dashed lines*), as measured by Hill and Stebbins (1975).

insensitive to the rotation rate in this region. Even with the rotation rate interior to M_r^* increased by a factor of 10, we find that the predicted oblateness is within the 1σ level if $M_r^* \lesssim 0.07\ M_\odot$. Such a rotation rate would, in fact, be required to substantially reduce the predicted neutrino flux, and the primary problem is how to produce such rapid rotation from a reasonable evolutionary scenario. An initial model with $\omega \propto \tilde{\omega}^{-2}$ (see § II*a*) *might* provide such rapid core rotation.

c) *Changes in Envelope Composition due to Rotational Mixing*

The circulation currents and instabilities which redistribute angular momentum within the stellar interior also mix the chemical composition. Although such mixing has often been invoked to explain surface composition anomalies (cf. Paczyński 1973; Sweigart and Mengel 1979), we are not aware of any previous calculations in which the effects of nucleosynthesis and mixing have been treated consistently, within an evolutionary sequence. In our models, simultaneous nucleosynthesis and mixing of ^{1}H, ^{3}He, ^{4}He, ^{12}C, ^{13}C, and ^{14}N were calculated from the modified diffusion equations (9).

Rotational mixing should not produce significant changes in the internal distribution of ^{1}H and ^{4}He because of the strong μ-barriers associated with gradients in the abundances of these nuclei. However, our calculations show that major changes in the distribution of the other nuclei (particularly ^{3}He and ^{13}C) can be caused by such mixing. The distribution of these elements in the models at an age of 4.7×10^9 yr is shown in Figure 8. The distribution in the sequence B model is shown by solid lines. Dash-dot and dashed lines are used for sequences A and C, where the profiles differ significantly from those of sequence B. Only the core profiles are shown for ^{12}C and ^{14}N since very little core-envelope mixing of these nuclei occurred.

As the figure shows, the envelopes of the more rapidly rotating models are well mixed down to the ^{3}He peak associated with partial *pp*-chain processing. (The ^{3}He profile in the sequence C model is nearly identical to the profile in a nonrotating model.) Since it is not possible to observe ^{3}He in solar type stars, this prediction cannot be directly tested. However, mixing of the chemical composition from the surface down to the ^{3}He peak also implies that the surface abundances of lithium and beryllium will be altered. The temperature at the ^{3}He peak is 7.3×10^6 K, whereas lithium and beryllium are destroyed at temperatures exceeding 3×10^6 K and 4×10^6 K, respectively. Thus, the observed surface abundances of these elements should provide an important check on our models. Unfortunately, mixing of lithium and beryllium was not calculated in our present models. Since the surface abundances are very sensitive to the degree of mixing (i.e., how many times the envelope "turns over"), as well as the depth of mixing, it is hazardous to guess how much dilution of lithium and beryllium will take place. (The ^{3}He profiles show that homogenization of the envelopes is far from complete.) Mixing of lithium and beryllium will be included in future model calculations, so we prefer not to speculate on what the predicted abundances will be.

Figure 8 also shows that, in the rapidly rotating models (sequence A), some mixing of the ^{13}C produced by partial CN-cycle processing occurred. In this case, almost all of the mixing took place during the first 10^9 yr of the evolution, before the μ-barrier was established at the C^{13} peak. (Since the μ-barrier never reaches the ^{3}He peak, the surface ^{3}He abundance changes continuously over the entire lifetime of the star.) In addi-

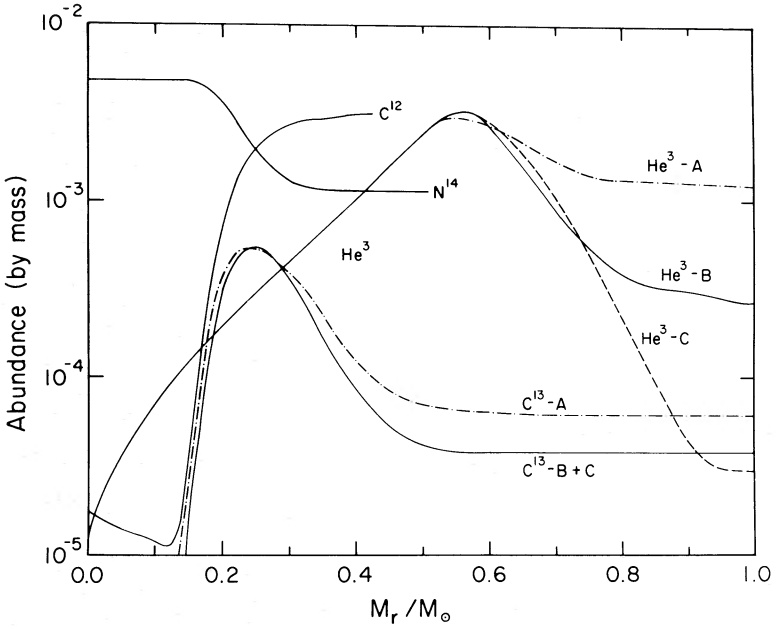

FIG. 8.—Internal abundance profiles in the models at an age of 4.7×10^9 yr. Solid lines are used for the sequence B profiles. The sequence A and C profiles are shown by dash-dot and dashed lines, if they differ significantly from the sequence B profiles.

tion to the model sequences discussed previously, we also computed a sequence with an initial angular momentum 9.76 times greater than the value given by equation (3). Since the surface velocity in this sequence comes very close (within 1%) to the critical velocity during the evolution to the ZAMS, this sequence should represent an upper limit on rotation among solar type stars. The changes in the surface abundances in all of our rotating sequences at age $=4.7\times10^9$ yr are given in Table 2. Since the ^{13}C mixing is confined to the early parts of the main-sequence stage, the $^{12}C/^{13}C$ ratios given in Table 2 should also hold for the end of the main-sequence stage.

In red giants which have evolved from solar type stars and are ascending the red giant branch for the first time, the observed surface $^{12}C/^{13}C$ ratios are often anomalous in the sense that they are much lower than predicted by nonrotating stellar evolution calculations. This problem has been reviewed in some detail by Dearborn, Eggleton, and Schramm (1976), and we will adopt the observed values in their Table 1 in the following discussion. A solar type star evolving up the red giant branch for the first time will develop a deep convective envelope, which will mix the ^{13}C peak out to the surface. However, because the mass in the ^{13}C peak is small compared to the total mass of the convective envelope, the ^{13}C is highly diluted, and this sets a definite limit on how much the $^{12}C/^{13}C$ ratio at the surface can be altered by such deep convection. For an initial ratio of 89 (the solar value), Dearborn *et al.* find that the final $^{12}C/^{13}C$ ratio should always be greater than 25, while stars that appear to be on the first ascent of the red giant branch have observed ratios varying from 50 to 12. Even with initial $^{12}C/^{13}C$ ratios as low as 40 (which Dearborn *et al.* consider a lower limit), final values lower than 20 cannot be produced in standard models of stars on the first ascent of the red giant branch. As a possible solution, they suggest that much of the envelope mass is lost prior to the onset of deep convection, thereby reducing the dilution of the

TABLE 2

SURFACE ABUNDANCE CHANGES AT AGE $=4.7\times10^9$ YEARS

$J_i/\langle J\rangle_i$	$^3He/^3He_i$	$^{12}C/^{12}C_i$	$^{13}C/^{13}C_i$	$^{14}N/^{14}N_i$	$^{12}C/^{13}C^a$
9.76.....	52.9	0.978	2.71	1.01	29.7
3.38(a)....	41.5	0.992	1.63	1.00	50.2
1.00(b)....	9.01	1.00	1.00	1.00	81.8
0.33(c)....	1.05	1.00	1.00	1.00	82.4

[a] $(^{12}C/^{13}C)_i = 82.4$

^{13}C peak. However, the implied mass loss rates are extremely large, requiring that ~10% of the kinetic energy flux of convection be put directly into the stellar wind. While a 10% efficiency is robust for almost any physical process, it is orders of magnitude greater than the conversion efficiency in the case of the solar wind, so this must be considered a desperate solution. (We should note that in models with double shell sources [second ascent of the red giant branch], $^{12}C/^{13}C$ ratios as low as 3.5 can be produced. However, these models apply only to the most luminous red giants, which are excluded from the present discussion.)

Our models suggest a more satisfactory solution to the problem of $^{12}C/^{13}C$ ratios in the less luminous red giants. Because of meridional circulation, the envelopes of our more rapidly rotating models are already enriched in ^{13}C when they leave the main sequence. This has the same effect as a low initial $^{12}C/^{13}C$ ratio, and we can use Figure 4 of Dearborn *et al.* to estimate the surface composition after deep convective mixing. For the initial $^{12}C/^{13}C$ ratio of 82 used in our models, we find final ratios ranging from 28 to 18 (depending on the intial rotation rate) in 1 $M_\odot$ stars. While a few of the observed values lie below this range, two additional considerations should further decrease the lower end of the predicted range. First, the final values will be lower for more massive stars (~2 $M_\odot$) because the ^{13}C peak occupies a larger fraction of the envelope mass. Second, the discussion in § IV*b* suggests that our present models underestimate the degree of mixing due to circulation currents.

It appears that most or all of the range of $^{12}C/^{13}C$ ratios can be explained without requiring large variations in the initial ratios or extreme mass loss rates. In addition, our models nicely explain ratios as low as 30, observed in red giants which have luminosities too low to have undergone deep convective mixing. Finally, we should note that our models do not predict significant changes in the $^{12}C/^{14}N$ ratio (see Table 2). This is because the μ-barrier is very effective in the region where the CN cycle approaches equilibrium and depletes a significant fraction of the ^{12}C. This is in agreement with the observed $^{12}C/^{14}N$ ratios and removes the primary objection to rotational mixing expressed by Dearborn *et al.* and Dearborn and Eggleton (1977).

V. CONCLUSIONS

Because our models fail to match the observed solar oblateness, we cannot claim to have correctly modeled the rotational history of the Sun. In addition, we cannot determine (from our present models) how much depletion of lithium and beryllium would result from the deep envelope circulation predicted by our models. Therefore, some caution must be exercised in interpreting our results. Nevertheless, we believe that the following conclusions, based on the results described in § IV, are warranted.

1. Models of solar-type stars, which have large initial angular momenta and which subsequently lose angular momentum due to a solar wind, have surface rotational velocities in the observed ranges for both pre–main-sequence and main-sequence stars. This supports the conclusion that the difference between the mean rotational velocities of lower- and upper-main-sequence stars is due to the action of magnetically coupled, solar type winds, rather than differences in the initial angular momenta.

2. The μ-barriers created by nuclear reactions deep in the solar core can inhibit circulation currents and stabilize differential rotation at a very early stage (i.e., at the ZAMS). In the absence of alternate angular momentum transport mechanisms, a rapidly rotating core could survive to the present age of the Sun. The core rotation would not, however, be rapid enough to significantly suppress the neutrino flux, if rigid-body rotation is the proper initial condition.

3. The circulation currents and instabilities which transport angular momentum within the stellar interior will also mix the chemical composition. In a typical solar type star (i.e., average initial angular momentum), these currents will bring ^3He-rich material up to the surface and increase the surface $^3He/^4He$ ratio. This may also explain the observed depletion of lithium, though our calculations cannot yet provide a quantitative estimate of this effect. Among the more rapidly rotating solar type stars, rotational mixing can produce significant increases of the ^{13}C abundance in the envelopes. Allowing for the uncertainties in our circulation model, it appears that the entire range of surface $^{12}C/^{13}C$ ratios observed in stars on the first ascent of the red giant branch can be explained by this mechanism.

We should also consider the possible causes and consequences of our failure to correctly match the observed solar oblateness. In § IV*b*, we suggested that this was due to a breakdown of our local diffusion model in regions with large gradients in the circulation velocities. Such gradients occur where the rotational velocity decreases dramatically within a narrow region. This breakdown seems, at first, surprising in view of the success of our diffusion model in predicting the surface rotational velocities of more massive stars evolving off the main sequence (Endal and Sofia 1979). However, these stars are not subject to strong external torques (the solar wind), so large gradients in the velocities do not occur in those early stages to which the observational checks apply. Thus, the solar case provides a test of the diffusion model under rather different conditions. In the massive stars, large gradients do develop as a result of core spin-up in the late stages of

evolution, and, if we have correctly identified the problem with the solar oblateness matching, some of our earlier conclusions about core spin-up in massive stars (Endal and Sofia 1977) may have to be modified.

We should keep in mind that fluid flows are not the only possible mechanisms for transporting angular momentum within a stellar interior. Our failure to match the solar oblateness may be due to neglect of these other mechanisms, rather than to a breakdown of our model for the circulation flows. For instance, we have not included the effects of magnetic fields. Because the interior of the Sun is an excellent conductor, the dynamo field generated in the envelope should not penetrate deeply into the radiative core. However, the region in our models where the large angular velocity gradients occur is quite shallow (see Fig. 6), and it is possible that the dynamo field plays a role at this depth. In fact, it is tempting to speculate that the interaction of differential rotation and turbulence in this region may actually drive the $\alpha\omega$-dynamo mechanism. This would be consistent with Parker's (1975) estimates of the magnetic buoyancy time scale.

It may be possible to distinguish between angular momentum transport by fluid flows and transport by other mechanisms by comparing predicted and observed surface abundances of lithium and beryllium. Fluid flows will be accompanied by chemical mixing while magnetic fields will not produce such mixing. Nonradial oscillations provide another mechanism for transporting angular momentum without chemical mixing (cf. Gough 1978). Thus, lithium and beryllium abundances in solar type stars may provide a crucial test of our models, and we expect to include these elements in future calculations.

APPENDIX A

DEFINITION OF THE ZERO-AGE MAIN SEQUENCE

The ZAMS at a given mass is conventionally defined by a chemically homogeneous model with no gravitational or thermal energy sources. This is a convenient starting point for an evolutionary sequence, since the Vogt-Russell theorem then ensures a unique solution to the stellar structure equations and this solution can be obtained (for a nonrotating model) without knowledge of the prior evolution. However, calculations started before the main-sequence stage show that the ZAMS is a computational, rather than a physical, concept in the sense that a real star never achieves a chemically homogeneous, static state. Nuclear reactions start prior to the main-sequence stage, and the gravitational and thermal energy sources do not go to zero in the entire star at the same time.

The approach to the main sequence, for a 1 $M_\odot$ star, has been described in detail by Iben (1965), and we will not repeat his description here. However, since we use the term ZAMS to specify a certain point in our evolutionary sequences, a definition of this term and some brief discussion is necessary. We operationally define the ZAMS as the point in the evolution where the radius of the star reaches its last minimum in approaching the main hydrogen-burning phase. Iben offers two alternative definitions, based on the minimum luminosity and the minimum rate of gravitational energy change. In a 1 $M_\odot$ star, minimum radius is reached first, followed by minimum luminosity and, last, by minimum energy change. Since the ZAMS is not a physically real concept, the choice of definition is not crucial as long as the definition is clearly stated. With our definition and starting from a luminosity of 25 $L_\odot$, the ZAMS is reached at an age of 4.46×10^7 yr in a nonrotating sequence.

The qualitative behavior of our nonrotating models is the same as described by Iben. However, there are quantitative differences due to improvements in the input physics (nuclear reactions and opacities). Starting from a luminosity of 16 $L_\odot$, Iben's models reach the minimum luminosity point after 3.38×10^7 yr. Our models have an age of 4.79×10^7 yr at this point. The difference in the initial luminosity is not significant since our models require only 2.25×10^4 yr to go from 25 to 16 $L_\odot$. Another difference concerns the size of the convective core which develops during the approach to the main sequence. In Iben's models, this core attains a maximum size of 0.11 $M_\odot$, while the convective core in our models only reaches 0.076 $M_\odot$.

A final consideration is the effect of the starting point on models of the present Sun (at an age of 4.7×10^9 yr). To investigate this, we computed an evolutionary sequence starting from a conventional ZAMS model and ending with a solar (1 $L_\odot$, 1 $R_\odot$) model after 4.7×10^9 yr. Comparison with the sequence started prior to the main sequence shows that the differences are insignificant. The change in the initial hydrogen content required to match the Sun is only 0.01%, the change in the mixing length is 4%, and the difference in the predicted neutrino fluxes is 1%. Although it is not necessary to start prior to the main sequence in a nonrotating sequence, this is not true for our rotating sequences (see § II*a*).

APPENDIX B

CALCULATION OF THE SURFACE OBLATENESS AND QUADRUPOLE MOMENT

The surface oblateness values listed in Table 1 and displayed in Figure 7 were calculated by assuming that the surface rotates rigidly and that magnetic fields do not change the surface shape. With these assumptions, equation (2) gives the relationship between the oblateness and the gravitational quadrupole moment (Dicke 1970). The quadrupole moment was calculated by integrating the standard second-order differential equation, derived by perturbation methods. This equation and the appropriate boundary conditions have been given in several earlier papers (Goldreich and Schubert 1968; Fricke 1969), and they will not be repeated here. We may note that the equation is usually stated without reference to a derivation; a very nice derivation is offered by Roxburgh (1964).

There is apparently some controversy regarding solutions to the quadrupole moment equation. For an identical rotation law $\omega(r)$, Fricke (1969) obtained a J_2 which was 3.5 times smaller than the value given by Goldreich and Schubert (1968). Fricke was unable to find the source of the discrepancy and attributed it to a numerical error in the Goldreich and Schubert calculation. We calculated J_2 for the same rotation law by several independent methods (Hamming's predictor-corrector, Runga-Kutta, Simpson's rule) and, in each case, obtained a value in agreement with Goldreich and Schubert. Further, for the alternate rotation law proposed by Fricke, we computed a J_2 value 2 times larger than Fricke. (This alternate rotation law implied slower rotation at a given r, so the discrepancy is systematic.) It appears that the error lies in Fricke's calculation.

The values given in Table 1 and Figure 7 were calculated using the Hamming's method, with an internal integration accuracy of 1 part in 10^7 and an accuracy in matching the boundary conditions of 1 part in 10^5.

REFERENCES

Anderson, J. D., Kessey, M. S. W., Lau, E. L., Standish, E. M., Jr., and Newhall, X.X. 1978, *Acta Astr.* **5**, 43.
Bahcall, J. N. 1978, *Rev. Mod. Phys.*, **50**, 881.
Bahcall, J. N., and Moeller, C. P. 1969, *Ap. J.*, **155**, 511.
Belcher, J. W., and MacGregor, K. B. 1976, *Ap. J.*, **210**, 498.
Bernacca, P. L., and Perinotto, M. 1974, *Astr. Ap.*, **33**, 433.
Brandt, J. 1966, *Ap. J.*, **144**, 1221.
Brans, C., and Dicke, R. H. 1961, *Phys. Rev.*, **124**, 925.
Buff, J., Gerola, H., and Stellingwerf, R. F. 1979, *Ap. J.*, **230**, 839.
Cohen, M., and Kuhi, L. V. 1979, *Ap. J. (Letters)*, **227**, L105.
Colgate, S. A. 1968, *Ap. J. (Letters)*, **153**, L81.
Davis, R., Jr. 1978, in *Proceedings, Solar Neutrino Conference-Brookhaven 1978*, ed. G. Friedlander (BNL 50879, Vol. 1), p. 1.
Dearborn, D. S. P., and Eggleton, P. P. 1977, *Ap. J.*, **213**, 177.
Dearborn, D. S. P., Eggleton, P. P., and Schramm, D. N. 1976, *Ap. J.*, **203**, 455.
Demarque, P., Mengel, J. G., and Sweigart, A. V. 1973, *Ap. J.*, **183**, 997.
Demarque, P., and Roeder, R. 1967, *Ap. J.*, **147**, 1188.
Dicke, R. H. 1970, *Ap. J.*, **159**, 1.
Dicke, R. H., and Goldenberg, H. M. 1967, *Phys. Rev. Letters*, **18**, 313.
Durney, B. R., and Latour, J. 1978, *Geophys. Ap. Fluid Dynamics*, **9**, 241.
Durney, B. R., and Spruit, H. C. 1979, *Ap. J.*, **234**, 1067.
Endal, A. S., and Sofia, S. 1976, *Ap. J.*, **210**, 184.
_____. 1977, *Phys. Rev. Letters*, **39**, 1429.
_____. 1978, *Ap. J.*, **220**, 279.
_____. 1979, *Ap. J.*, **232**, 531.
_____. 1980, in *Conference on the Ancient Sun*, ed. R. P. Pepin and J. A. Eddy (New York: Pergamon Press), in press.
Fowler, W. A., Caughlan, G. R., and Zimmerman, B. A. 1975, *Ann. Rev. Astr. Ap.*, **13**, 69.
Fricke, K. 1969, *Ap. Letters*, **3**, 219.
Goldreich, P., and Schubert, G. 1967, *Ap. J.*, **150**, 571.
_____. 1968, *Ap. J.*, **154**, 1005.
Gough, D. O. 1978, in *Proceedings of the Workshop on Solar Rotation*, ed. G. Belvedere and L. Paterno (Osservatorio Astrofisico di Catania, Pub. No. 162), p. 87.
Hill, H. A., and Stebbins, R. T. 1975, *Ap. J.*, **200**, 471.
Huebner, W. F., Merts, A. L., Magee, N. H., Jr., and Argo, M. F. 1977, Los Alamos Scientific Laboratory publication LA-6760-M.
Iben, I., Jr. 1965, *Ap. J.*, **141**, 993.
James, R. A., and Kahn, F. D. 1970, *Astr. Ap.*, **5**, 232.
_____. 1971, *Astr. Ap.*, **12**, 332.
Kippenhahn, R. 1963, *Ap. J.*, **137**, 664.
_____. 1969, *Astr. Ap.*, **2**, 309.
Kraft, R. P. 1970, in *Spectroscopic Astrophysics*, ed. G. H. Herbig (Berkeley: University of California Press), p. 385.
Kuhi, L. V. 1978, *Moon and Planets*, **19**, 199.
Landolt, A. U. 1979, *Ap. J.*, **231**, 468.
Larson, R. B. 1969, *M.N.R.A.S.*, **145**, 271.
Moss, D. L. 1973, *M.N.R.A.S.*, **161**, 225.
Neugebauer, M., and Davies, R. W. 1978, *A Close-Up of the Sun* (JPL Publication 78-70).
Paczyński, B. 1973, *Acta Astr.*, **23**, 191.
Parker, E. N. 1975, *Ap. J.*, **198**, 205.
Rhodes, E. J. Jr., Deubner, F. L., and Ulrich, R. K. 1979, *Ap. J.*, **227**, 629.
Rosen, N. 1971, *Phys. Rev. D*, **3**, 2317.
Ross, J. E., and Aller, L. H. 1976, *Science*, **191**, 1223.
Roxburgh, I. W. 1964, *Icarus*, **3**, 92.
Sakurai, T. 1972, *Pub. Astr. Soc. Japan*, **24**, 153.
Shapiro, I. I. 1965, *Icarus*, **4**, 549.
Shapiro, I. I., Counselman, C. C., III, and King, R. W. 1976, *Phys. Rev. Letters*, **36**, 555; erratum on p. 1068 of same volume.
Skumanich, A. 1972, *Ap. J.*, **171**, 565.
Smith, M. A. 1979, *Pub. A.S.P.*, **91**, 737.
Sweigart, A. V., and Mengel, J. G. 1979, *Ap. J.*, **229**, 624.
Weber, E., and Davis, L. 1967, *Ap. J.*, **148**, 217.
Will, C. M., and Nordtvedt, K., Jr. 1972, *Ap. J.*, **177**, 757.
Williams, J. G., *et al.*, 1976, *Phys. Rev. Letters*, **36**, 551.
Wolff, C. L. 1976, Ap. J., **205**, 612.
Zahn, J.-P. 1975, *Mém. Soc. Roy. Sci. Liège*, **8**, 31.

A. S. ENDAL: Department of Physics and Astronomy, Louisiana State University, Baton Rouge, LA 70803

S. SOFIA: Code 961, Goddard Space Flight Center, Greenbelt, MD 20771